Noble metal-free, Ni-Zn-Al-based oxide/spinel nanostructures for high performance, methane-selective CO_2 hydrogenation reactions

T. Rajkumar[a], András Sápi[a,b,*], Marietta Ábel[a], Juan Fernando Gómez-Pérez[a], Ákos Kukovecz[a], Zoltán Kónya[a,c]

[a]*University of Szeged, Interdisciplinary Excellence Centre, Department of Applied and Environmental Chemistry, H-6720, Rerrich Béla tér 1, Szeged, Hungary*
[b]*Institute of Environmental and Technological Sciences, University of Szeged, H-6720, Szeged, Hungary*
[c]*MTA-SZTE Reaction Kinetics and Surface Chemistry Research Group, University of Szeged, H-6720, Szeged, Hungary*

∗Corresponding author at: University of Szeged, Interdisciplinary Excellence Centre, Department of Applied and Environmental Chemistry, H-6720, Rerrich Béla tér 1, Szeged, Hungary.

E-mail address: sapia@chem.u-szeged.hu (A. Sápi).

Abstract

In the present study, NiO modified $ZnAl_2O_4$ and ZnO modified $NiAl_2O_4$ spinel along with pure Al_2O_3, $ZnAl_2O_4$ and $NiAl_2O_4$ for comparison in the CO_2 hydrogenation reaction have been investigated. It was found that $NiAl_2O_4$, $NiO/ZnAl_2O_4$ and $ZnO/NiAl_2O_4$ catalysts exhibited outstanding activity and selectivity towards methane even at high temperature compared to similar spinel structures reported in the literature. $NiO/ZnAl_2O_4$ catalyst showed CO_2 consumption rate of ~ 19 μmol/g·s at 600 °C and ~ 85 % as well as ~ 50 % of methane selectivity at 450 °C and 600 °C, respectively. The high activity and selectivity of methane can be attributed to the presence of metallic Ni and $Ni/NiO/ZnAl_2O_4$ interface under the reaction conditions evidenced by ex-situ XRD results.

Introduction

Utilization of fossil fuels leads to CO_2 emission which in turn leads to global warming[1]. Currently, CO_2 hydrogenation is desirable strategy to not only reduce the CO_2 emission but also to produce useful chemicals/fuels[2, 3]. Depending upon the catalysts used, different kinds of products were obtained at ambient pressures such as CO (RWGS), methane (Sabatier reaction) and methanol[4-6]. In recent years, variety of catalytic materials have been studied for the above reactions. Among them Cu[7], Pt[8] and Rh[9] on various supports have been reported as the most active catalysts for reducing CO_2 to CO. Ni[10], Ru[5] and Rh[11] are most widely used

catalysts for CO_2 methanation reaction. Cu[12] and Pd[13] are most widely used catalysts for the reduction of CO_2 to methanol.

Spinel oxides have been used in various fields such as in catalysis[14], sensors[15] and refractory materials[16] due to their catalytic properties and thermal stability. Nickel aluminate ($NiAl_2O_4$) is has an inverse spinel structure with nickel ion occupies the octahedral site. $NiAl_2O_4$ were used in various fields such as in catalysis [17-20], adsorption[21], sensors[15] and as flexible materials[22]. They have also been used as catalyst support due to its low reactivity with the active phase and its high resistance to high temperatures and acidic or basic atmospheres[23]. Interestingly, $NiAl_2O_4$ was found to minimize the coke formation in CO_2 reforming of methane[24].

$ZnAl_2O_4$ is a normal spinel with all the zinc cations in the tetrahedral and all the aluminium cations in the octahedral sites of the cubic face-centered lattice of oxygen anions[25]. Zinc aluminate ($ZnAl_2O_4$) were used in various fields such as in catalysis[26-28], adsorption[29] and optics[30]. They have specific properties including low acidity and high thermal stability [31]. These features minimize the coke formation which leads to high product selectivity[32].

In this work, various Nickel-Zinc-Aluminum-based spinels as well as oxide/spinel catalysts were produced where the position of the nickel and zinc atoms or ions were changed. The catalysts were characterized by X-ray diffraction (XRD), N_2 physisorption and Transmission Electron Microscopy (TEM). These catalysts were tested in CO_2 hydrogenation reaction in the gas phase. It was found that $NiAl_2O_4$, $NiO/ZnAl_2O_4$ and $ZnO/NiAl_2O_4$ catalysts during the reaction conditions exhibited outstanding activity and selectivity towards methane even at high temperature as these catalysts presented metallic nanoparticles in their structure. Due to the presence of metallic nickel and $Ni/NO/ZnAl_2O_4$ interface under the reaction conditions, $NiO/ZnAl_2O_4$ catalyst showed CO_2 consumption rate of ~ 19 μmol/g·s at 600 °C and ~ 85 % as well as ~ 50 % of methane selectivity at 450 °C and 600 °C, respectively.

Results and discussion

X-ray diffraction (XRD)

The crystal structure of catalysts was investigated by XRD. Fig. 1 shows the XRD patterns of Al_2O_3, $NiAl_2O_4$, $ZnAl_2O_4$, $NiO/ZnAl_2O_4$ and $ZnO/NiAl_2O_4$. The peaks located at 2θ of 19.86°, 32.38°, 37.85°, 46.20°, 57.40°, 61.02° and 67.12° are assigned to (111), (220), (311), (400),

(422), (511) and (440) planes of the cubic structure of γ-Al_2O_3[33]. The peaks located at 2θ of 18.9°, 31.38°, 36.67°, 44.39° and 64.88° are assigned to the (111), (220), (311), (400) and (440) planes of the cubic spinel structure of $NiAl_2O_4$ respectively (JCPDS Card no. 73-0239)[34]. The peaks located at 2θ of 18.99°, 31.69°, 37.17°, 45.26°, 49.06°, 55.66°, 59.65°, 65.62°, 74.15° and 77.33° are assigned to the (111), (220), (311), (400), (331), (422), (511), (440), (620) and (536) planes of the cubic spinel structure of $ZnAl_2O_4$ respectively (JCPDS Card no. 05-0669)[27]. For $NiO/ZnAl_2O_4$ and $ZnO/NiAl_2O_4$ samples no peaks characteristics of ZnO and NiO are seen indicating fine dispersion of these species on the $NiAl_2O_4$ and $ZnAl_2O_4$ supports respectively or may be overlapped with the supports diffraction peaks.

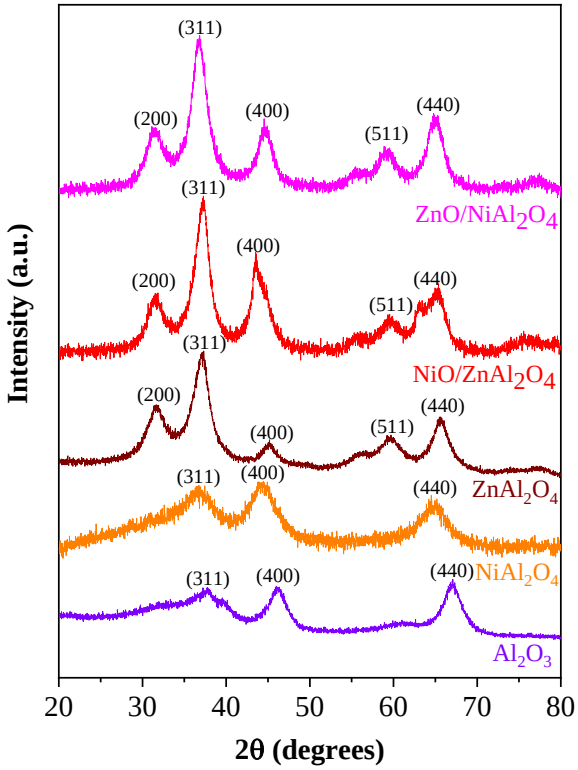

Fig. 1 XRD patterns of Al_2O_3, $NiAl_2O_4$, $ZnAl_2O_4$, $NiO/ZnAl_2O_4$ and $ZnO/NiAl_2O_4$ catalysts

N_2 adsorption-desorption isotherm

Fig. 2 shows the nitrogen adsorption-desorption isotherms and Fig. 3 shows corresponding pore size distribution of the catalysts. The characteristic specific surface area together with the pore volume and pore size was summarized in Table 1. The N_2 adsorption-desorption isotherms of $ZnO/NiAl_2O_4$ exhibit type IV isotherm with a narrow hysteresis loop of type H3 associated

with plate-like particles giving rise to slit-shaped pores[35]. However, Al_2O_3, $NiAl_2O_4$, $ZnAl_2O_4$ and $NiO/ZnAl_2O_4$ displays type IV isotherms with H2 hysteresis loop at P/P_0 = 0.4-1.0 associated with pores with narrow necks and wide bodies, referred to as 'ink-bottle' pores[35, 36]. The average pore size distribution is in the range of 2-25 nm indicating the presence of mesopores. After loading ZnO and NiO respectively on $NiAl_2O_4$ and $ZnAl_2O_4$, the resulting catalyst showed decreased surface area and pore volume.

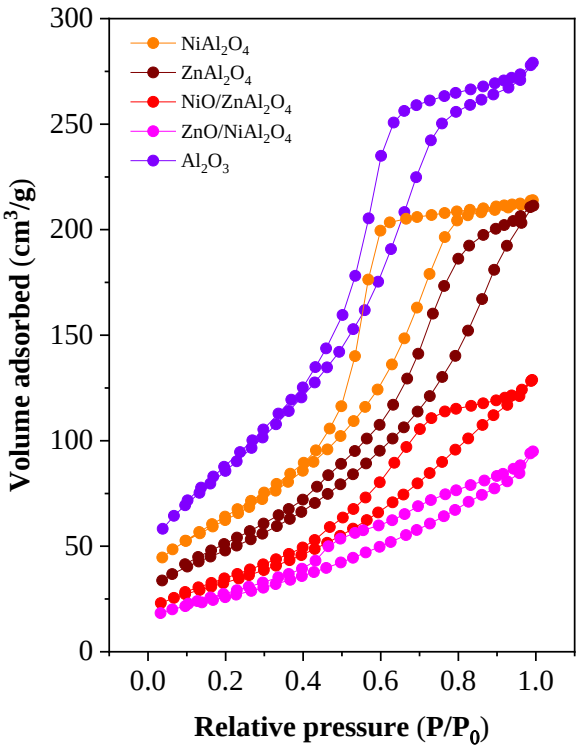

Fig. 2 N_2 adsorption-desorption isotherm of Al_2O_3, $NiAl_2O_4$, $ZnAl_2O_4$, $NiO/ZnAl_2O_4$ and $ZnO/NiAl_2O_4$ catalysts

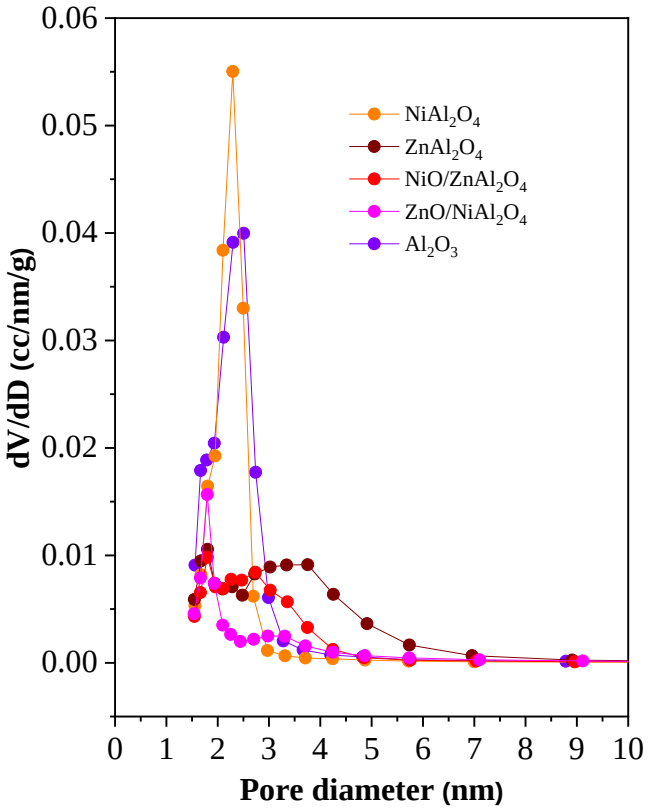

Fig. 3 Pore size distributions of Al_2O_3, $NiAl_2O_4$, $ZnAl_2O_4$, $NiO/ZnAl_2O_4$ and $ZnO/NiAl_2O_4$ catalysts

Table 1. Textural parameters of the catalysts

Samples	**BET surface area (m^2/g)**	**Pore volume (cm^3/g)**	**Average pore size (nm)**
Al_2O_3	321	0.42	2.51
$NiAl_2O_4$	226	0.33	2.29
$ZnAl_2O_4$	175	0.31	1.80
$NiO/ZnAl_2O_4$	120	0.19	1.80
$ZnO/NiAl_2O_4$	94	0.13	1.80

Transmission Electron Microscopy (TEM)

The morphology and particle size of the catalysts were examined by TEM measurements and shown in Fig. 4. $NiAl_2O_4$ shows spherical shaped morphology with the size of 10 to 20 nm. TEM images of the $NiO/ZnAl_2O_4$ and $ZnO/NiAl_2O_4$ catalysts show two separate phases of

metal oxides and supports that are well mixed and dispersed which is similar to what have been reported in the literature for $NiO/NiAl_2O_4$ catalyst[37].

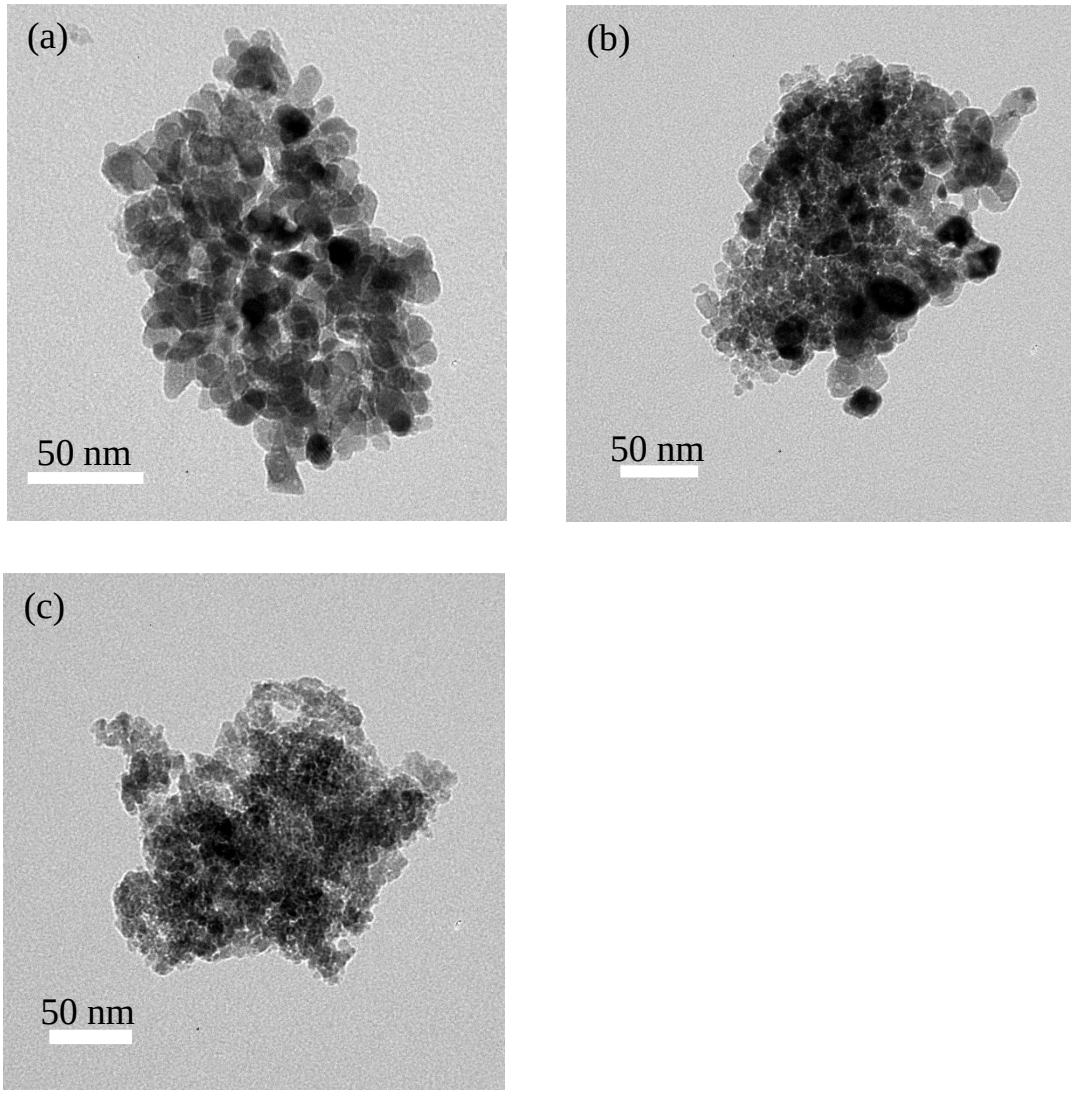

Fig. 4 TEM images of (a) $NiAl_2O_4$ (b) $NiO/ZnAl_2O_4$ (c) $ZnO/NiAl_2O_4$

Catalytic performances

To explore the catalytic performance, CO_2 hydrogenation was performed over the prepared catalysts. Fig. 5 depicts the CO_2 conversion as a function of temperature over all the catalysts. CO_2 conversion and product selectivity are given in Table 2 over all the catalysts. In general, the activity of Ni based catalysts are remarkably better than that of Zn-based catalysts and Al_2O_3 catalyst. $NiAl_2O_4$, $NiO/ZnAl_2O_4$ and $ZnO/NiAl_2O_4$ catalysts exhibit highest activity with CO_2 conversion of 65% at 600 °C, which is 2.8 fold superior in catalytic activity than that of

Al_2O_3 (Conversion = 23%) and 2 fold superior in catalytic activity than that of $ZnAl_2O_4$ (Conversion = 31%).

Fig. 6 depicts the selectivity as a function of temperature for all the studied catalysts. The CO selectivity increases with increasing temperature due to the endothermic RWGS reaction. Among the five systems (Al_2O_3, $NiAl_2O_4$, $ZnAl_2O_4$, $NiO/ZnAl_2O_4$ and $ZnO/NiAl_2O_4$) considered in this study, the Ni containing catalysts such as $NiAl_2O_4$, $NiO/ZnAl_2O_4$ and $ZnO/NiAl_2O_4$ produced CH_4 and CO as the product but the Zn containing catalysts such as $ZnAl_2O_4$ as well as Al_2O_3 produced CO as the only product. All the nickel-containing spinels and oxide/spinel structures showed a high selectivity towards methane even at high temperature. $NiO/ZnAl_2O_4$ system has a methane selectivity of ~ 85 % as well as ~ 50 % at 450 °C and 600 °C, respectively.

The CO_2 conversion exhibit a decrease in the order: < $NiO/ZnAl_2O_4$ < $NiAl_2O_4$ < $ZnO/NiAl_2O_4$ < $ZnAl_2O_4$ < Al_2O_3. This can be correlated with increasing Ni content. Given that an increase in Ni content can enhance CO_2 hydrogenation activity[38]. The $NiO/ZnAl_2O_4$ exhibited 65% CO_2 conversion at 600 °C with CH_4 and CO as the products. All of the Ni containing catalysts produce CH_4 as main products and CO as minor products while ZnO and other Zn containing catalysts as well as Al_2O_3 produce only CO.

In general, Ni based catalysts produce CH_4 through decomposition of formate species to CO and subsequent hydrogenation of adsorbed CO leads to the production of CH_4[39] and ZnO is more active for the RWGS reaction[40]. Table 3 lists the CO_2 consumption rates of all the catalysts studied at 600 °C. Fig. 7 depicts the CO_2 consumption rate as a function of temperature for all the studied catalysts. The CO_2 consumption rate is highest on $NiO/ZnAl_2O_4$, namely ca. 19.7 μmol h^{-1} g^{-1} at 600 °C which was 2.5 times higher than that of Al_2O_3 (ca. 7.9 μmol h^{-1} g^{-1} at 600 °C) catalyst. This catalyst also outperforms other reported spinel catalysts (Table 4) in the CO_2 hydrogenation reaction.

Although the surface area of Al_2O_3 was far higher than the $NiO/ZnAl_2O_4$, the CO_2 consumption rate was far higher on $NiO/ZnAl_2O_4$. This was due to presence of metallic Ni under reaction condition in $NiO/ZnAl_2O_4$ than in the other catalysts. Comparative table of CO_2 consumption rate of the catalyst in this study with the spinel catalyst reported in the literature for CO_2 hydrogenation is given in Table 4.

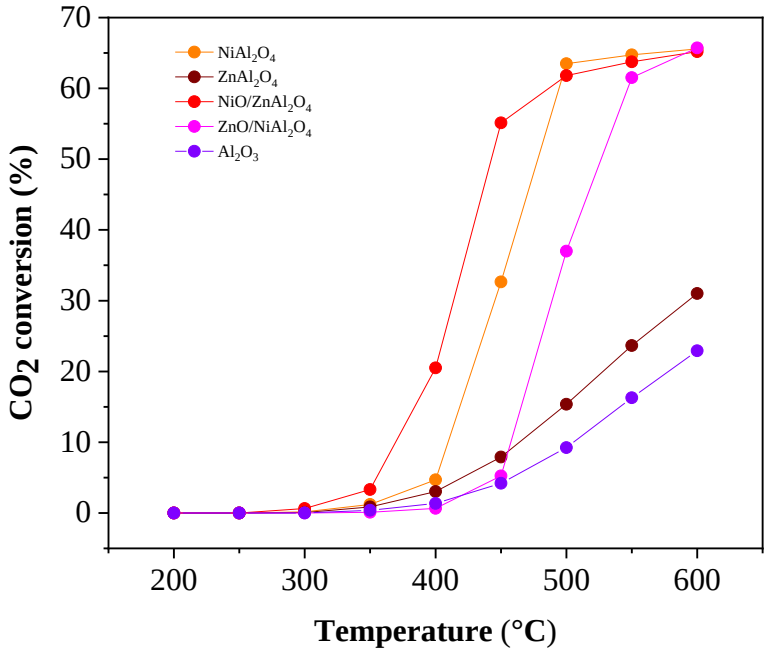

Fig. 5 CO_2 conversion as a function of temperature over Al_2O_3, $NiAl_2O_4$, $ZnAl_2O_4$, $NiO/ZnAl_2O_4$ and $ZnO/NiAl_2O_4$ catalysts

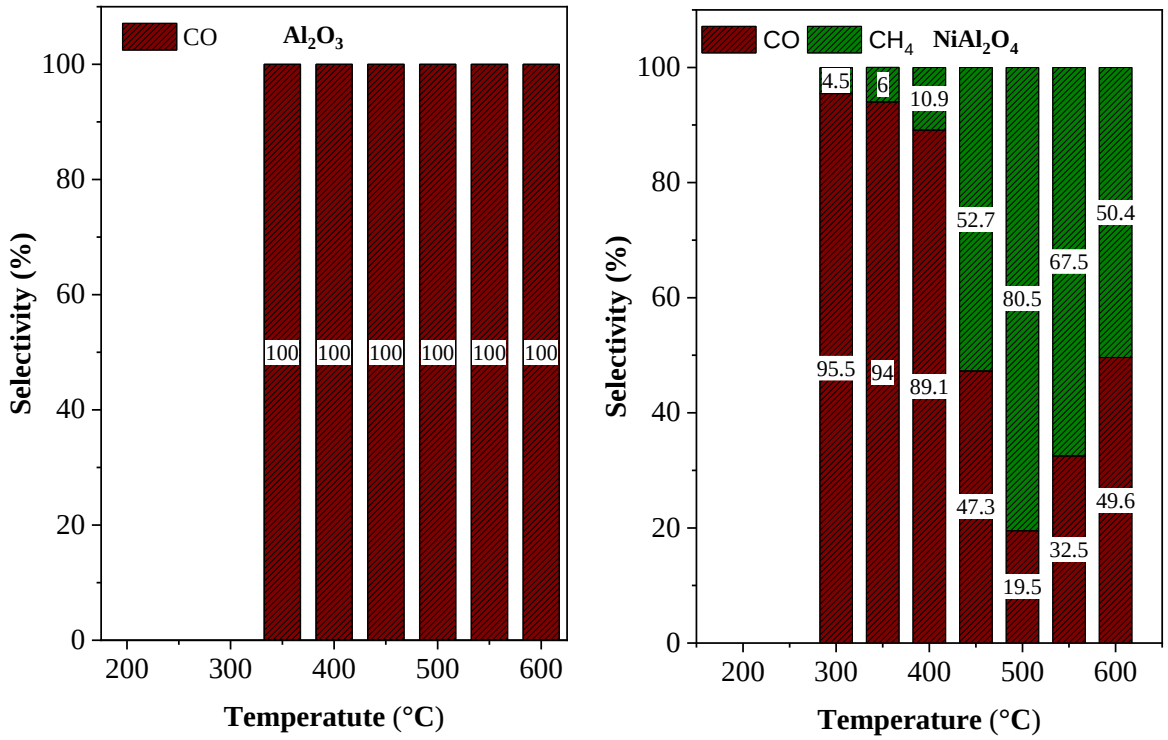

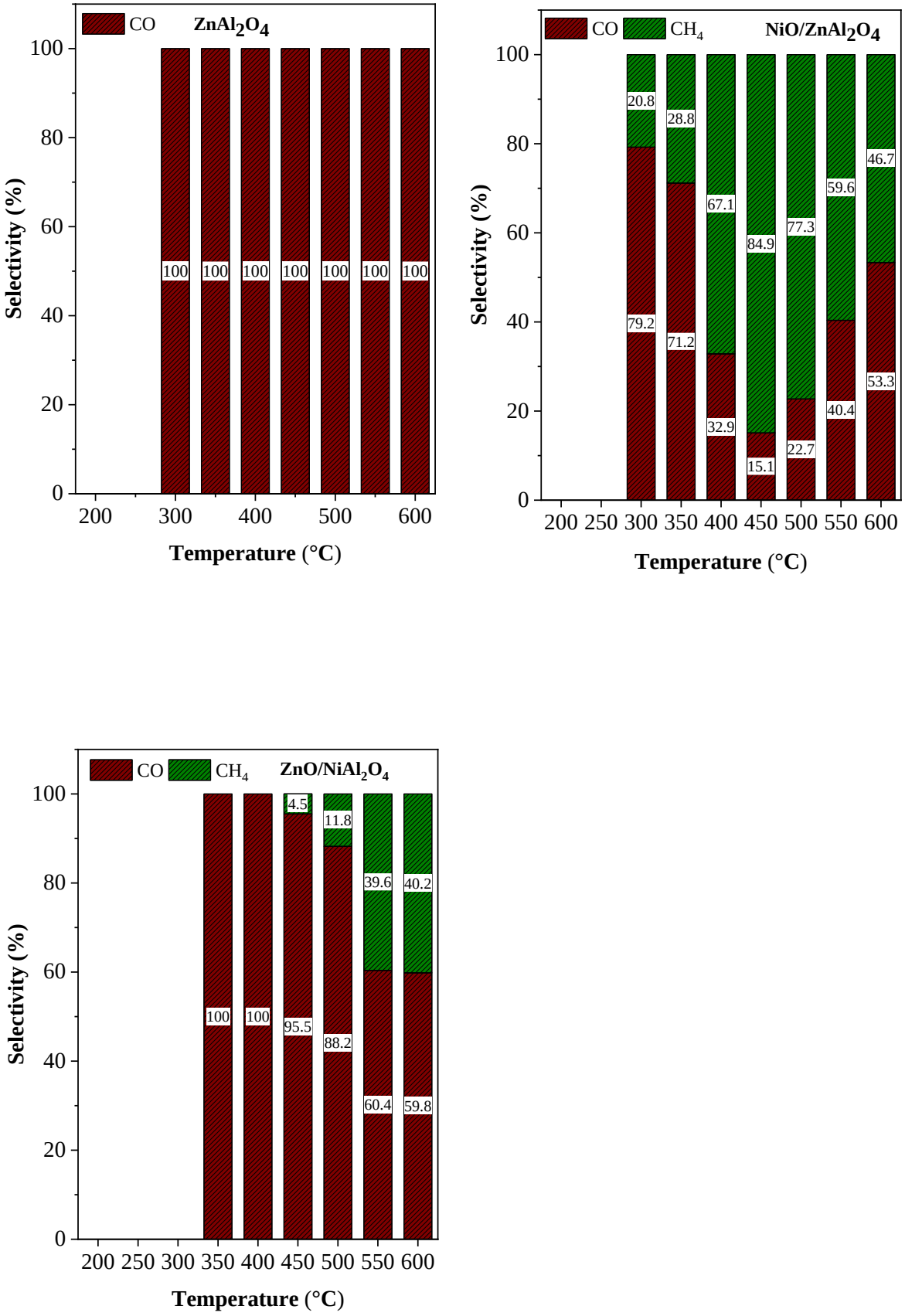

Fig. 6 Selectivity for the CO_2 hydrogenation over Al_2O_3, $NiAl_2O_4$, $ZnAl_2O_4$, $NiO/ZnAl_2O_4$ and $ZnO/NiAl_2O_4$ catalysts

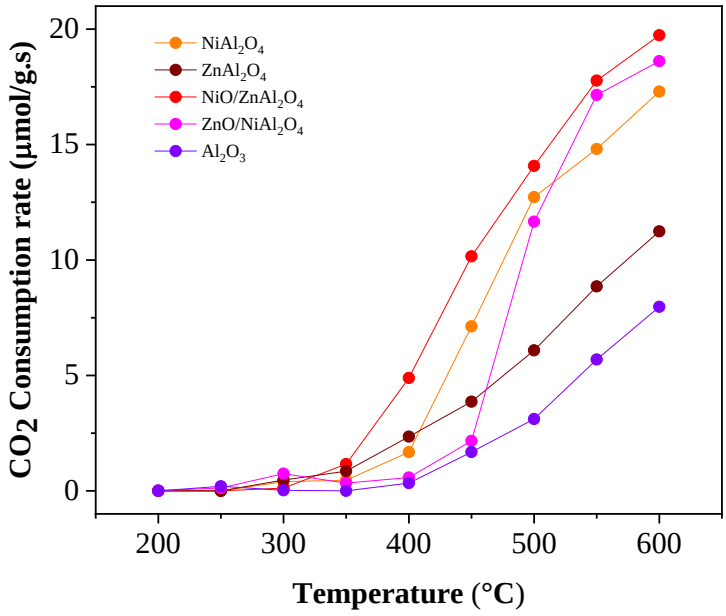

Fig. 7 CO_2 consumption rate as a function of temperature over Al_2O_3, $NiAl_2O_4$, $ZnAl_2O_4$, $NiO/ZnAl_2O_4$ and $ZnO/NiAl_2O_4$ catalysts

Table 2 Conversion and selectivity for CO_2 hydrogenation over various catalysts [a]

Catalysts	CO_2 Conversion (%)	Selectivity (%)	
		CO	CH_4
Al_2O_3	22.91	100	0
$NiAl_2O_4$	65.57	49.60	50.40
$ZnAl_2O_4$	31.02	100	0
$NiO/ZnAl_2O_4$	65.18	53.35	46.65
$ZnO/NiAl_2O_4$	65.71	59.83	40.17

[a] Reaction conditions: T = 600℃, CO_2/H_2 = 1/4, catalyst weight = 0.15g

Table 3. The CO_2 consumption rate (μmol/g.s) at 600 °C in CO_2 hydrogenation reaction over Al_2O_3, $NiAl_2O_4$, $ZnAl_2O_4$, $NiO/ZnAl_2O_4$ and $ZnO/NiAl_2O_4$ catalysts

Catalysts	CO_2 consumption rate (μmol/g.s)
Al_2O_3	7.97
$NiAl_2O_4$	17.29
$ZnAl_2O_4$	11.23
$NiO/ZnAl_2O_4$	19.73
$ZnO/NiAl_2O_4$	18.61

Table 4 Comparative table of CO_2 consumption rate with the reported spinel catalyst for CO_2 hydrogenation

Catalysts	CO_2 conversion (%)	Catalyst Weight (g)	Temperature (°C)	Flow rate of CO_2 (ml/s)	CO_2 consumption rate (μmol/g.s)	References
$NiO/ZnAl_2O_4$	65	0.15	600	0.17	19.730	This work
$0.08wt\%Na/ZnFe_2O_4$	34	1	340	0.13	1.807	[41]
Co_3O_4 spinel	48	1	450	0.17	3.335	[42]
$Fe(2+)[Fe(3+)_{0.5}Al_{0.5}]_2O_4$ spinel	40	1	320	0.12	1.962	[43]
$Cu_xZn_{1x}Al_2O_4$ spinel	4	1	250	0.42	0.687	[44]
$ZnFeO_x$-nNa	39	0.5	320	0.28	8.927	[45]
Cu–Zn–Al/SAPO-34	33	0.5	400	0.19	5.126	[46]
$ZnGa_2O_4$/SAPO-34	37	0.5	450	0.19	5.747	[46]

Characterization of spent catalysts

The spent catalysts were studied by XRD to elucidate the structural changes. The XRD of spent catalysts after catalytic test are displayed in Fig. 8. All Ni containing spent catalysts show peaks in addition to fresh ones at $2\theta = 45.39°$, 52.62° and 77° corresponding to the (111), (200) and (220) planes attributed to the metallic nickel (JCPDS No. 04-0850)[47]. However Zn containing

spinels and Al_2O_3 spent catalysts showed almost no changes in their crystalline phases indicating that their crystal structures are more stable during the reaction.

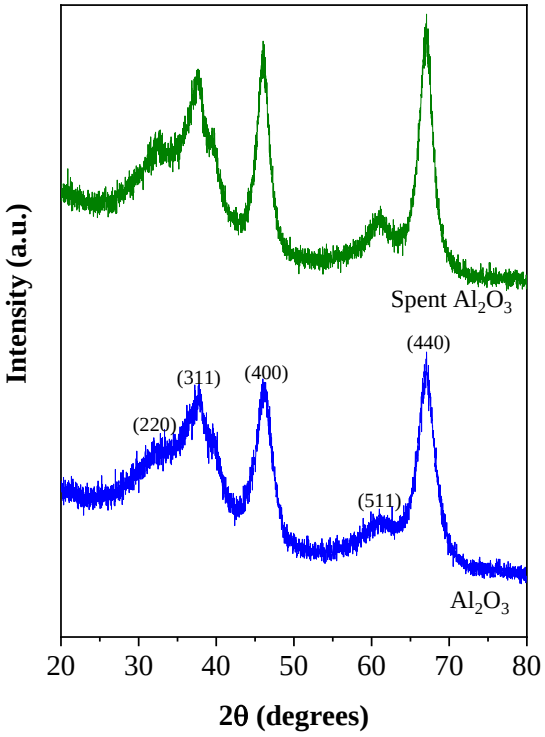

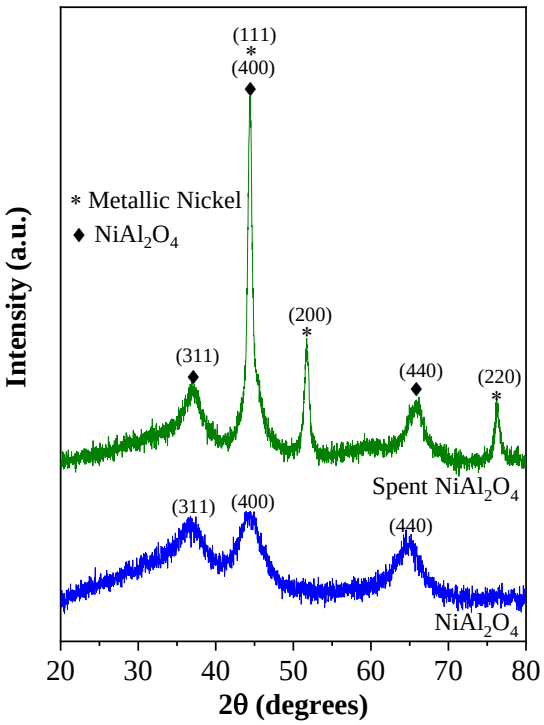

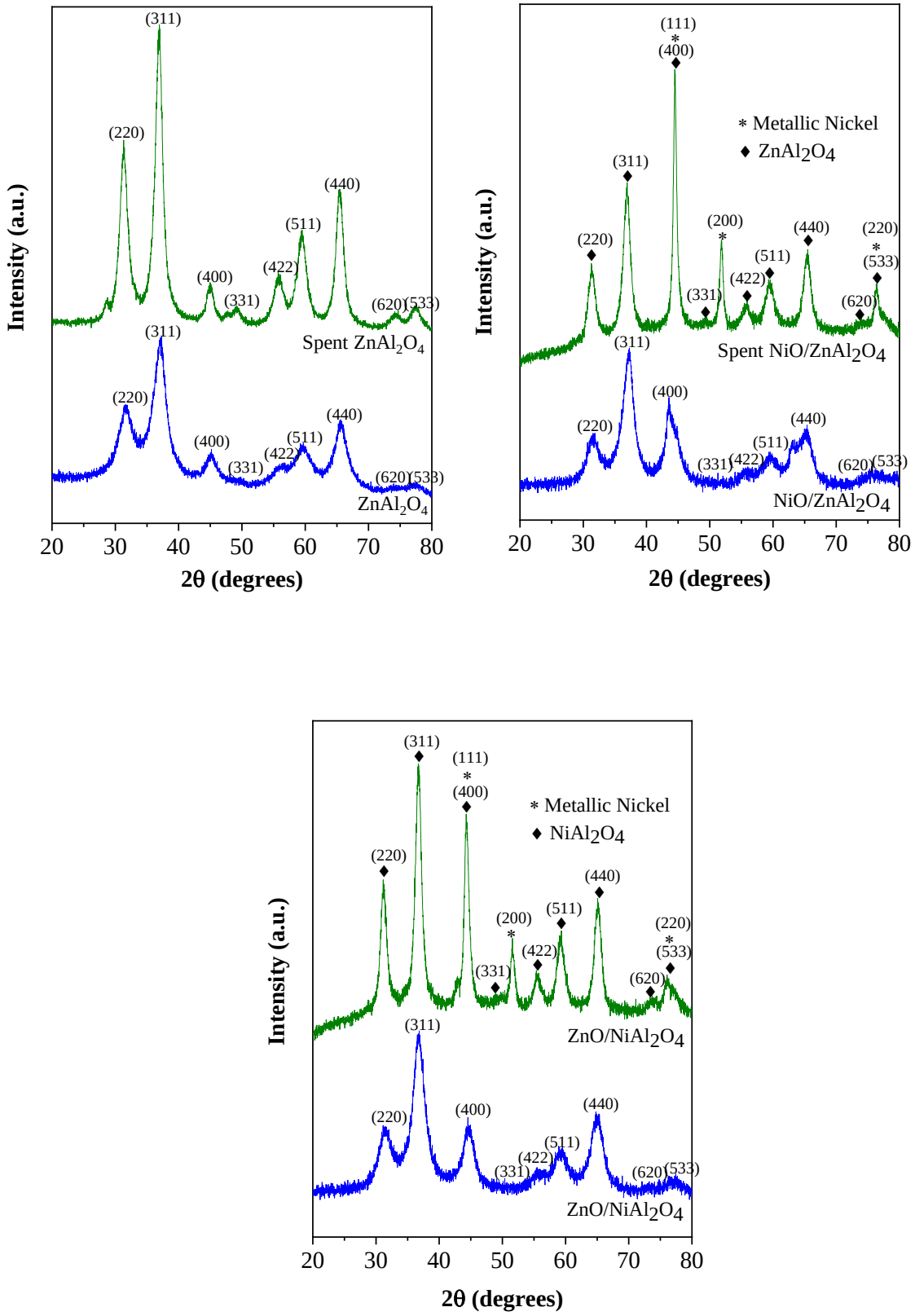

Fig. 8 XRD profiles of spent catalysts after catalytic test

Conclusion

CO_2 hydrogenation over Al_2O_3, $NiAl_2O_4$, $ZnAl_2O_4$, $NiO/ZnAl_2O_4$ and $ZnO/NiAl_2O_4$ catalysts have been investigated and it was found that $NiAl_2O_4$, $NiO/ZnAl_2O_4$ and $ZnO/NiAl_2O_4$ catalysts exhibit high activity with CO_2 conversion of 65% at 600 °C, which is several times more active compared to other catalysts reported in the literature. On the other hand, these catalysts showed a high methane selectivity even at high temperatures. The higher catalytic activity and CH_4 selectivity of $NiAl_2O_4$, $NiO/ZnAl_2O_4$ and $ZnO/NiAl_2O_4$ catalysts can be attributed to the presence of metallic Ni under the reaction conditions which can enhance the CO_2 hydrogenation activity.

Experimental details

Chemicals

$Zn(NO_3)_2{\cdot}6H_2O$ (≥ 99%) and $Al(NO_3)_3{\cdot}9H_2O$ (≥ 98%) were purchased from Sigma-Aldrich. Aqueous ammonia solution was purchased from Molar chemicals. $Ni(NO_3)_2{\cdot}6H_2O$ was purchased from Merck.

Catalyst preparation

The $ZnAl_2O_4$ oxide was synthesized by a co-precipitation method in accordance with the procedure reported in the previous work[48]. Typically, appropriate amount of $Zn(NO_3)_2{\cdot}6H_2O$ and $Al(NO_3)_3{\cdot}9H_2O$ with a molar ratio of 1:2 were dissolved in 100 mL deionized water. Then, an aqueous ammonia solution was added dropwise into the mixed solution at room temperature until pH value of about 7. The obtained precipitate was aged for 2 h at 70 °C. Then, the solid product was recovered by filtration, washing with deionized water and drying overnight at 100 °C. The $ZnAl_2O_4$ was obtained after calcination in air at 500 °C for 5 h. The $NiAl_2O_4$ and pure Al_2O_3 were prepared by the same procedure using their corresponding metal nitrate precursors. In order to investigate the interphase effect of metal cations present in the $ZnAl_2O_4$ and $NiAl_2O_4$ spinels, we loaded exactly the amount of ZnO present in $ZnAl_2O_4$ onto $NiAl_2O_4$ and vice versa. Based on the calculation, we loaded 44wt% of ZnO on $NiAl_2O_4$ and represented as $ZnO/NiAl_2O_4$ and 42wt% of NiO on $ZnAl_2O_4$ and represented as $NiO/ZnAl_2O_4$.

Catalyst Characterization

N_2 adsorption-desorption isotherm measurements

The specific surface area (BET method), the pore size distribution and the total pore volume were determined by the BJH method using a Quantachrome NOVA 2200 gas sorption analyzer by N_2 gas adsorption/desorption at -196 °C. Before the measurements, the samples were pre-treated in a vacuum (<~0.1 mbar) at 200 °C for 2 hours.

Powder X-ray Diffraction (XRD)

XRD studies of all samples were performed on a Rigaku MiniFlex II instrument with a Ni-filtered CuKα source in the range of $2\theta = 10\text{-}80°$.

Transmission Electron Microscopy (TEM)

Imaging of the all the samples were carried out using an FEI TECNAI G2 20 X-Twin high-resolution transmission electron microscope (equipped with electron diffraction) operating at an accelerating voltage of 200 kV. The samples were drop-cast onto carbon film coated copper grids from ethanol suspension.

Catalytic activity studies

Hydrogenation of carbon-dioxide in a continuous flow reactor

Before the catalytic experiments, the as-received catalysts were oxidized in O_2 atmosphere at 300 °C for 30 min and thereafter were reduced in H_2 at 300 °C for 60 min. Catalytic reactions were carried out at atmospheric pressure in a fixed-bed continuous-flow reactor (200 mm long with 8 mm i.d.) which was heated externally. The dead volume of the reactor was filled with quartz beads. The operating temperature was controlled by a thermocouple placed inside the oven close to the reactor wall, to assure precise temperature measurement. For catalytic studies, small fragments (about 1 mm) of slightly compressed pellets were used. Typically, the reactor filling contained 150 mg of catalyst. In the reacting gas mixture, the CO_2: H_2 molar ratio was 1:4, if not denoted otherwise. The CO_2: H_2 mixture was fed with the help of mass flow controllers (Aalborg), the total flow rate was 50 ml/min. The reacting gas mixture flow entered and left the reactor through an externally heated tube in order to avoid condensation. The analysis of the products and reactants was performed with an Agilent 6890 N gas chromatograph using HP-PLOTQ column. The gases were detected

simultaneously by thermal conductivity (TC) and flame ionization (FI) detectors. The CO_2 was transformed by a methanizer to methane and it was also analysed by FID. CO_2 conversion was calculated on a carbon atom basis, i.e.

$$\mathrm{CO_2\ conversion(\%)} = \frac{\mathrm{CO_{2\ inlet} - CO_{2\ outlet}}}{\mathrm{CO_{2\ inlet}}} \times 100\%$$

CH_4 selectivity and CO selectivity were calculated as following

$$\mathrm{CH_4\ selectivity(\%)} = \frac{\mathrm{CH_{4\ outlet}}}{\mathrm{CO_{2\ inlet} - CO_{2\ outlet}}} \times 100\%$$

$$\mathrm{CO\ selectivity(\%)} = \frac{\mathrm{CO_{\ outlet}}}{\mathrm{CO_{2\ inlet} - CO_{2\ outlet}}} \times 100\%$$

where $\mathrm{CO_{2\ inlet}}$ and $\mathrm{CO_{2\ outlet}}$ represent the $\mathrm{CO_2}$ concentration in the feed and effluent, respectively, and $\mathrm{CH_{4\ outlet}}$ and $\mathrm{CO_{\ outlet}}$ represent the concentration of $\mathrm{CH_4}$ and CO in the effluent, respectively.

Acknowledgement

This paper was supported by the Hungarian Research Development and Innovation Office through grants NKFIH OTKA PD 120877 of AS. AK, and KZ is grateful for the fund of NKFIH (OTKA) K112531 & NN110676 and K120115, respectively. The financial support of the Hungarian National Research, Development and Innovation Office through the GINOP-2.3.2-15-2016-00013 project "Intelligent materials based on functional surfaces - from syntheses to applications" and the Ministry of Human Capacities through the EFOP-3.6.1-16-2016-00014 project and the, grant 20391-3/2018/FEKUSTRAT is acknowledged.

Keywords: Spinel, Co-precipitation method, XRD, CO_2 hydrogenation

References

[1] G. A. Florides, P. Christodoulides *Environment international*. **2009**, *35*, 390-401.
[2] W. Wang, S. Wang, X. Ma, J. Gong *Chemical Society Reviews*. **2011**, *40*, 3703-3727.
[3] S. Roy, A. Cherevotan, S. C. Peter *ACS Energy Letters*. **2018**, *3*, 1938-1966.
[4] X. Zhang, X. Zhu, L. Lin, S. Yao, M. Zhang, X. Liu, X. Wang, Y.-W. Li, C. Shi, D. Ma *ACS Catal.* **2016**, *7*, 912-918.
[5] F. Wang, S. He, H. Chen, B. Wang, L. Zheng, M. Wei, D. G. Evans, X. Duan *J. Am. Chem. Soc.* **2016**, *138*, 6298-6305.
[6] M. M.-J. Li, C. Chen, T. c. e. Ayvalı, H. Suo, J. Zheng, I. F. Teixeira, L. Ye, H. Zou, D. O'Hare, S. C. E. Tsang *ACS Catal.* **2018**, *8*, 4390-4401.
[7] E. L. Fornero, D. L. Chiavassa, A. L. Bonivardi, M. A. Baltanás *J. CO2 Util.* **2017**, *22*, 289-298.

[8] X. Chen, X. Su, H. Duan, B. Liang, Y. Huang, T. Zhang *Catalysis today*. **2017**, *281*, 312-318.
[9] L. Dietz, S. Piccinin, M. Maestri *The Journal of Physical Chemistry C*. **2015**, *119*, 4959-4966.
[10] W. WANG, C. Duong-Viet, H. Ba, W. Baaziz, G. Tuci, S. Caporali, L. Nguyen-Dinh, O. Ersen, G. Giambastiani, C. Pham-Huu *ACS Applied Energy Materials*. **2018**.
[11] H. Arandiyan, K. Kani, Y. Wang, B. Jiang, J. Kim, M. Yoshino, M. Rezaei, A. E. Rowan, H. Dai, Y. Yamauchi *ACS applied materials & interfaces*. **2018**, *10*, 24963-24968.
[12] B. Rungtaweevoranit, J. Baek, J. R. Araujo, B. S. Archanjo, K. M. Choi, O. M. Yaghi, G. A. Somorjai *Nano Lett.* **2016**, *16*, 7645-7649.
[13] H. Bahruji, M. Bowker, G. Hutchings, N. Dimitratos, P. Wells, E. Gibson, W. Jones, C. Brookes, D. Morgan, G. Lalev *Journal of Catalysis*. **2016**, *343*, 133-146.
[14] L. Zhou, Y. Guo, J.-M. Basset, H. Kameyama *Chem. Commun.* **2015**, *51*, 12044-12047.
[15] J. J. Vijaya, L. J. Kennedy, G. Sekaran, B. Jeyaraj, K. Nagaraja *J. Hazard. Mater.* **2008**, *153*, 767-774.
[16] Y. Chen, G. Liu, W. Zhen, Y. Zhang, B. Fan, R. Zhang, H. Li *J Alloys Compd*. **2019**, *770*, 356-368.
[17] C. Jiménez-González, Z. Boukha, B. de Rivas, J. R. González-Velasco, J. I. Gutiérrez-Ortiz, R. n. López-Fonseca *Energy & Fuels*. **2014**, *28*, 7109-7121.
[18] X. Yan, C. Yuan, J. Bao, S. Li, D. Qi, Q. Wang, B. Zhao, T. Hu, L. Fan, B. Fan *Catalysis Science & Technology*. **2018**.
[19] B. Valle, N. García-Gómez, A. Arandia, A. Remiro, J. Bilbao, A. G. Gayubo *Int J Hydrogen Energy*. **2019**.
[20] A. Morales-Marín, J. Ayastuy, U. Iriarte-Velasco, M. Gutiérrez-Ortiz *Appl. Catal. B Environ.* **2019**, *244*, 931-945.
[21] N. Salleh, A. Jalil, S. Triwahyono, J. Efendi, R. Mukti, B. Hameed *Appl Surf Sci*. **2015**, *349*, 485-495.
[22] M. A. Rahman, E. Ahamed, M. R. I. Faruque, M. T. Islam *Sci. Rep.* **2018**, *8*, 14948.
[23] A. L. García-Lario, M. Aznar, I. Martinez, G. S. Grasa, R. Murillo *Int J Hydrogen Energy*. **2015**, *40*, 219-232.
[24] Y. Kathiraser, W. Thitsartarn, K. Sutthiumporn, S. Kawi *The Journal of Physical Chemistry C*. **2013**, *117*, 8120-8130.
[25] M. Nasr, R. Viter, C. Eid, F. Warmont, R. Habchi, P. Miele, M. Bechelany *RSC Adv*. **2016**, *6*, 103692-103699.
[26] F. Le Peltier, P. Chaumette, J. Saussey, M. Bettahar, J. Lavalley *J. Mol. Catal. A Chem.* **1998**, *132*, 91-100.
[27] J. Liu, W. Zhou, D. Jiang, W. Wu, C. Miao, Y. Wang, X. Ma *Industrial & Engineering Chemistry Research*. **2018**, *57*, 11265-11270.
[28] A. Wang, J. Wang, C. Lu, M. Xu, J. Lv, X. Wu *Fuel*. **2018**, *234*, 430-440.
[29] L. Zhao, S. Bi, J. Pei, X. Li, R. Yu, J. Zhao, C. J. Martyniuk *J. Ind. Eng. Chem.* **2016**, *41*, 151-157.
[30] W. Mulwa, B. Dejene, M. Onani, C. Ouma *Journal of Luminescence*. **2017**, *184*, 7-16.
[31] J. Okal, M. Zawadzki *Appl Catal A Gen*. **2013**, *453*, 349-357.
[32] S. A. Bocanegra, A. Guerrero-Ruiz, S. R. de Miguel, O. A. Scelza *Appl Catal A Gen*. **2004**, *277*, 11-22.
[33] J. Sun, Y. Wang, H. Zou, X. Guo, Z.-j. Wang *Journal of Energy Chemistry*. **2019**, *29*, 3-7.
[34] Y. Sun, E. Jiang, X. Xu, J. Wang, Z. Li *ACS Sustainable Chemistry & Engineering*. **2018**, *6*, 14660-14668.
[35] K. S. Sing *Pure Appl. Chem.* **1985**, *57*, 603-619.

[36] F. R. Shamskar, M. Rezaei, F. Meshkani *Int J Hydrogen Energy*. **2017**, *42*, 4155-4164.
[37] C. Wang, Y. Chen, Z. Cheng, X. Luo, L. Jia, M. Song, B. Jiang, B. Dou *Energy & Fuels*. **2015**, *29*, 7408-7418.
[38] C. Heine, B. A. Lechner, H. Bluhm, M. Salmeron *J. Am. Chem. Soc.* **2016**, *138*, 13246-13252.
[39] X. Jia, X. Zhang, N. Rui, X. Hu, C.-j. Liu *Appl. Catal. B Environ.* **2019**, *244*, 159-169.
[40] S.-W. Park, O.-S. Joo, K.-D. Jung, H. Kim, S.-H. Han *Appl Catal A Gen*. **2001**, *211*, 81-90.
[41] Y. H. Choi, E. C. Ra, E. H. Kim, K. Y. Kim, Y. J. Jang, K. N. Kang, S. H. Choi, J. H. Jang, J. S. Lee *ChemSusChem*. **2017**, *10*, 4764-4770.
[42] H. Kierzkowska-Pawlak, P. Tracz, W. Redzynia, J. Tyczkowski *J. CO2 Util.* **2017**, *17*, 312-319.
[43] N. Utsis, R. Vidruk-Nehemya, M. Landau, M. Herskowitz *Faraday discussions*. **2016**, *188*, 545-563.
[44] F. Conrad, C. Massue, S. Kühl, E. Kunkes, F. Girgsdies, I. Kasatkin, B. Zhang, M. Friedrich, Y. Luo, M. Armbrüster *Nanoscale*. **2012**, *4*, 2018-2028.
[45] X. Cui, P. Gao, S. Li, C. Yang, Z. Liu, H. Wang, L. Zhong, Y. Sun *ACS Catal.* **2019**, *9*, 3866-3876.
[46] X. Liu, M. Wang, C. Zhou, W. Zhou, K. Cheng, J. Kang, Q. Zhang, W. Deng, Y. Wang *Chem. Commun.* **2018**, *54*, 140-143.
[47] S. Song, S. Yao, J. Cao, L. Di, G. Wu, N. Guan, L. Li *Appl. Catal. B Environ.* **2017**, *217*, 115-124.
[48] W. Zhou, J. Kang, K. Cheng, S. He, J. Shi, C. Zhou, Q. Zhang, J. Chen, L. Peng, M. Chen *Angewandte Chemie*. **2018**, *130*, 12188-12192.